

# Superconductivity in Li-B-C system at 100 GPa

Feng Zheng<sup>1</sup>, Yang Sun<sup>2,3\*</sup>, Renhai Wang<sup>4</sup>, Yimei Fang<sup>1</sup>, Feng Zhang<sup>2,5</sup>, Shunqing Wu<sup>1†</sup>, Cai-Zhuang Wang<sup>2,5</sup>, Vladimir Antropov<sup>2,5</sup>, Kai-Ming Ho<sup>2</sup>

<sup>1</sup>*Department of Physics, OSED, Key Laboratory of Low Dimensional Condensed Matter Physics (Department of Education of Fujian Province), Jiujiang Research Institute, Xiamen University, Xiamen 361005, China.*

<sup>2</sup>*Department of Physics, Iowa State University, Ames, Iowa 50011, United States*

<sup>3</sup>*Department of Applied Physics and Applied Mathematics, Columbia University, New York, NY, 10027, USA*

<sup>4</sup>*School of Physics and Optoelectronic Engineering, Guangdong University of Technology, Guangzhou 510006, China*

<sup>5</sup>*Ames Laboratory, U.S. Department of Energy, Ames, Iowa 50011, USA*

## Abstract

Layer Li-B-C compounds have been shown to have feasible superconductivity. Using the adaptive genetic algorithm, we predict the structures of the Li-B-C system at 100 GPa. We identify several low-enthalpy metallic phases with stoichiometries of LiB<sub>2</sub>C, LiB<sub>3</sub>C, Li<sub>2</sub>BC<sub>2</sub>, Li<sub>3</sub>B<sub>2</sub>C<sub>3</sub>, Li<sub>3</sub>BC, and Li<sub>5</sub>BC. Using a fast screening method of electron-phonon interaction, we find that LiB<sub>3</sub>C is a promising candidate for superconductivity. The consecutive calculations using the full Brillouin zone confirm the existence of the strong electron-phonon coupling in this system. The anharmonic B-C phonon modes near the zone center provide the major contribution to the electron-phonon coupling. The electron-phonon coupling constant is 1.40, and the estimated critical temperature is 22 K. Our study indicates superconductivity can also happen without a layered structural motif in the Li-B-C system. It also demonstrates an effective strategy for crystal structure prediction of superconducting materials.

---

\*yangsun@iastate.edu

†wsq@xmu.edu.cn

## 1. Introduction

Exploring high-temperature superconductors is an important research goal in physics, chemistry, and material science. Inspired by the discovery of a superconducting transition around 40 K in the rather simple  $\text{MgB}_2$  compound [1-3], extensive research has been conducted on its related materials [4-9] (graphitelike layered materials intercalated with alkali or alkali-earth) to obtain new possible superconductors. Among them, graphitelike layered Li-B-C compounds have been the subject of sustained interest, because these structures with light elements may have strong covalent bonding and significant phonon frequencies, underling high- $T_c$  (conventional) superconductivity [10, 11]. LiBC with  $P6_3/mmc$  symmetry [12, 13] has a similar crystal structure to  $\text{MgB}_2$ . However, unlike  $\text{MgB}_2$ , LiBC exhibits an insulating nature [13]. According to Bardeen-Cooper-Schrieffer (BCS) theory [14], metallicity is an important requirement for a conventional superconductor. Therefore, to achieve superconductivity in LiBC, Rosner *et al.* suggested metalizing LiBC by introducing vacancies at Li sites [15]. Based on the DFT calculations, they found that  $\text{Li}_{0.5}\text{BC}$  becomes superconducting at about 100 K. However, no experimental efforts have reported superconductivity of the Li-deficient LiBC compounds above 2 K [16-19]. Further research shows that the absence of superconductivity of  $\text{Li}_x\text{BC}$  can be attributed to structural instability in the B-C layer at low Li deficiency, which leads to a dramatic change in electronic structure [20]. Considering that hole doping by introducing Li vacancies will cause structural instability in  $\text{Li}_x\text{BC}$ , Gao *et al.* designed a freestanding  $\text{LiB}_2\text{C}_2$  trilayer [5]. Due to no vacancies involved in trilayer  $\text{LiB}_2\text{C}_2$ , the structural distortion in the B-C layer may be prevented. And first-principles calculations predict that this trilayer  $\text{LiB}_2\text{C}_2$  is a superconductor with  $T_c$  about 92 K. Furthermore, partially replacing carbons with borons in LiBC-type compounds was also proposed, such as  $\text{LiB}_{1.1}\text{C}_{0.9}$  [21],  $\text{Li}_3\text{B}_4\text{C}_2$  [22],  $\text{Li}_2\text{B}_3\text{C}$  [22] and  $\text{Li}_4\text{B}_5\text{C}_3$  [7], which have all been predicted to be superconductors. More recently, Quan *et al.* reported the superconductivity in the honeycomb structure  $\text{Li}_{2x}\text{BC}_3$  at  $x = 0.5$  by the theoretical calculations [23]. The calculated superconducting critical temperature  $T_c$  is comparable

to that in  $\text{MgB}_2$ . These results show that the design of stoichiometric constituents of graphitelike layered Li-B-C compounds provides a feasible route to induce superconductivity.

So far, most attention has been focused on elucidating the nature of superconductivity of Li-B-C compounds with a graphitelike layered structure. A natural question remains whether there is any other Li-B-C structure that can lead to superconductivity. To answer this question, a comprehensive investigation of the crystal structures and superconductivity of the Li-B-C system should be carried out. These studies can help establish correlations of structural stability and superconducting properties with different structural motifs in the Li-B-C system, which, in turn, can be used to guide other researchers to reveal more promising superconductors. On the other hand, it has been shown that high pressure offers another effective strategy for identifying structural motifs for superconductivity [24-27]. Because high pressure conditions can enhance the interatomic interaction, tune electronic properties, and metalize materials. Furthermore, the application of pressure also can access unusual chemistry and stable structures that cannot be realized under ambient conditions [28], which may raise the possibility of finding superconducting materials. Therefore, in this paper, we investigate the structural and superconducting properties of the Li-B-C system at 100 GPa with crystal structure predictions. We employ a recently developed frozen-phonon method of electron-phonon coupling calculations [29] to fast screen possible Li-B-C superconductors.

## 2. Computational methods

The crystal structures of B-C, Li-C, and Li-B-C at 100 GPa were determined by using the [adaptive genetic algorithm \(AGA\)](#) method [30], which combines fast structure exploration by auxiliary classical potentials and accurate *ab initio* calculations adaptively and iteratively. In the GA-loop, the initial atomic position of the Li, B and C atoms were randomly generated without any assumption on the Bravais lattice type, symmetry, atom basis, or unit cell dimensions. The total structure pool in our GA search was set to 128. The structure search with auxiliary interatomic potentials was performed

in 400 consecutive GA generations. Then, the 16 lowest-enthalpy structures at the end of each GA search were selected for single-point DFT calculations according to the AGA procedure [30], whose energies, force, and stress are used to adjust the interatomic potential parameters for the next iteration of GA search. A total of 40 adaptive iterations were performed to obtain the final structures.

Here, the embedded-atom method (EAM) [31] was used as classical auxiliary potential. In EAM, the total energy of an  $N$ -atom system was evaluated by

$$E_{total} = \frac{1}{2} \sum_{i,j(i \neq j)}^N \phi(r_{ij}) + \sum_i F_i(n_i), \quad (1)$$

where  $\phi(r_{ij})$  denotes the pair repulsion between atoms  $i$  and  $j$  with a distance of  $r_{ij}$ ,  $F_i(n_i)$  is the embedded term with electron density term  $n_i = \sum_{j \neq i} \rho_j(r_{ij})$  at the site occupied by atom  $i$ . The potential fitting is performed by the force-matching method with a stochastic simulated annealing algorithm as implemented in the POTFIT code [32, 33].

The first-principles calculations were performed by using the projector-augmented wave (PAW) [34] representations with density functional theory as implemented in the Vienna *ab initio* simulation package (VASP) [35, 36]. The exchange and correlation energy was treated within the spin-polarized generalized gradient approximation (GGA) and parameterized by Perdew-Burke-Ernzerhof (PBE) formula [37]. Wave functions were expanded in plane waves up to a kinetic energy cutoff of 520 eV. Brillouin-zone integrations were approximated using special  $k$ -point sampling of the Monkhorst-Pack scheme [38] with a  $k$ -point mesh resolution of  $2\pi \times 0.03 \text{\AA}^{-1}$ . Lattice vectors and atomic coordinates were fully relaxed until the force on each atom was less than  $0.01 \text{ eV} \cdot \text{\AA}^{-1}$ . The fast screening of electron-phonon coupling (EPC) constant  $\lambda_{\Gamma}$  at the Brillouin zone center was carried out based on the frozen-phonon method [29]. The zone-center phonon was computed by the PHONOPY software [39, 40], with a finer  $k$ -point sampling grid of  $2\pi \times 0.02 \text{\AA}^{-1}$  spacing and a criterion of self-consistent calculation  $10^{-8} \text{ eV}$ .

The full Brillouin-zone EPC calculation were performed with the Quantum ESPRESSO (QE) code [41, 42] based on density-functional perturbation theory

(DFPT) [43]. The ultra-soft pseudopotentials from the PSLibrary1.0.0 (high accuracy) [44] for PBE functional were used, with  $2s^1$ ,  $2s^22p^1$ , and  $2s^22p^2$  as valence electrons of Li, B, and C, respectively. The kinetic energy cutoffs were 75 Ry for wave functions and 576 Ry for potentials. The charge densities were determined on a  $k$  mesh of  $24 \times 24 \times 24$ . The dynamical matrices were calculated on a  $q$  mesh of  $6 \times 6 \times 6$ . The convergence threshold for self-consistency was  $1 \times 10^{-12}$  Ry.

The calculations of superconducting  $T_c$  are based on the Eliashberg spectral equation  $\alpha^2F(\omega)$  [45, 46] defined commonly now as

$$\alpha^2F(\omega) = \frac{1}{2\pi N(E_f)} \sum_{qv} \frac{\gamma_{qv}}{\hbar\omega_{qv}} \delta(\omega - \omega_{qv}), \quad (2)$$

where  $N(E_f)$  is the density of states at the Fermi level,  $\omega_{qv}$  denotes the phonon frequency of the mode  $v$  with wave vector  $\mathbf{q}$ .  $\gamma_{qv}$  is the phonon linewidth defined as

$$\gamma_{qv} = \frac{2\pi\omega_{qv}}{\Omega_{BZ}} \sum_{ij} \int d^3k |g_{k,qv}^{ij}|^2 \delta(\epsilon_{q,i} - E_f) \delta(\epsilon_{k+q,j} - E_f), \quad (3)$$

where  $\epsilon_{q,i}$  and  $\epsilon_{k+q,j}$  are eigenvalues of Kohn-Sham orbitals at given bands and vectors.  $\mathbf{q}$  and  $\mathbf{k}$  are wave vectors, and  $i$  and  $j$  denote indices of energy bands.  $g_{k,qv}^{ij}$  is the EPC matrix element, which describes the probability amplitude for the scattering of an electron with a transfer of crystal momentum  $\mathbf{q}$ , determined by

$$g_{k,qv}^{ij} = \left(\frac{\hbar}{2M\omega_{qv}}\right)^{1/2} \left\langle \Psi_{i,k} \left| \frac{dV_{SCF}}{d\hat{\mu}_{qv}} \cdot \hat{e}_{qv} \right| \Psi_{i,k+q} \right\rangle, \quad (4)$$

where  $M$  is the atomic mass,  $\hat{e}_{qv}$  is the phonon eigenvector.  $dV_{SCF}/d\hat{\mu}_{qv}$  measures the change of self-consistent potential induced by atomic displacement.  $\Psi_{i,k}$  and  $\Psi_{i,k+q}$  are Kohn-Sham orbitals. The EPC constant  $\lambda$  can be determined through summation over the first Brillouin zone or integration of the spectral function in frequency space,

$$\lambda = \sum_{qv} \lambda_{qv} = 2 \int \frac{\alpha^2F(\omega)}{\omega} d\omega, \quad (5)$$

where the EPC constant  $\lambda_{qv}$  for mode  $v$  at wave vector  $\mathbf{q}$  using Eq. (5) can be written as

$$\lambda_{qv} = \frac{\gamma_{qv}}{\pi\hbar N(E_f)\omega_{qv}^2}. \quad (6)$$

The superconducting  $T_c$  is determined with the analytical McMillan equation modified by the Allen-Dynes formula [47, 48],

$$T_c = \frac{\omega_{log}}{1.2} \exp \left[ \frac{-1.04(1+\lambda)}{\lambda(1-0.62\mu^*)-\mu^*} \right], \quad (7)$$

where  $\mu^*$  is the effective screened Coulomb repulsion constant whose values is generally between 0.1 and 0.15 [49, 50], and  $\omega_{log}$  is the logarithmic average frequency

$$\omega_{log} = \exp \left[ \frac{2}{\lambda} \int \frac{d\omega}{\omega} \alpha^2 F(\omega) \log \omega \right]. \quad (8)$$

### 3. Results and discussion

#### 3.1 AGA search of Li-B-C ternary phases at 100 GPa

Before we discuss ternary compounds in the Li-B-C system, the structural stability of elements and binary phases should be first clarified. At 100 GPa, calculations show that the ground-state phases of elemental Li, B and C adopt the *Pbca* [51, 52], *Cmca* ( $\alpha$ -Ga structure) [53] and *Fd $\bar{3}m$*  (diamond) [54] symmetry, respectively. For the Li-B binary phase, because previous crystal structure searches [55, 56] have already covered the current study's pressure, we did not perform additional structure searches of Li-B compounds. We re-calculated the enthalpies of these crystal structures. Our results show that five compounds with  $\text{Li}_6\text{B}$  (*R $\bar{3}$* ),  $\text{Li}_2\text{B}$  (*Cmcm*),  $\text{Li}_3\text{B}_2$  (*R $\bar{3}m$* ),  $\text{LiB}$  (*Fd $\bar{3}m$* ) and  $\text{LiB}_4$  (*I4/mmm*) are stable at 100 GPa. For the B-C compounds, Jay *et al* investigated from ambient pressure to 80 GPa [57]. We performed the AGA search at 100 GPa and found no B-C binary compound was stable at 100 GPa, similar to Jay *et al.*'s high-pressure results [57]. For the Li-C system, our AGA searches indicate that  $\text{Li}_4\text{C}$  (*P2 $_1$ /c*),  $\text{Li}_8\text{C}_3$  (*R $\bar{3}m$* ) and  $\text{Li}_2\text{C}_3$  (*Cmcm*) compounds are the ground-state phases at 100 GPa. More details of AGA searches in B-C and Li-C systems can be found in Supplemental Materials. The stable crystal structures of these elements and binary phases are shown in Figure S3 and their structural parameters are listed in Supplementary Table S1.

In Figure 1, we present ternary compounds of Li-B-C at 100 GPa from the AGA searches. For simplicity, all chemical formulae are expressed as Li/B/C reduced ratios. For example, 111 represents the compound with  $\text{LiBC}$ . During the structural search, we select a range of different stoichiometries (i.e., 111, 112, 121, 211, 113, 122, 131, 212, 221, 311, 114, 123, 132, 141, 213, 231, 312, 321, 411, 115, 124, 133, 142, 151, 214,

223, 232, 241, 313, 322, 331, 412, 421, 511, 116, 125, 134, 143, 152, 161, 215, 233, 251, 314, 323, 332, 341, 413, 431, 512, 521 and 611) with 2 or 4 formula units to perform the AGA search. The relative stability of these predicted Li-B-C compounds was investigated under the corresponding pressure, depending on the calculated formation enthalpies,

$$H_f = \frac{H(\text{Li}_x\text{B}_y\text{C}_z) - xH(\text{Li}) - yH(\text{B}) - zH(\text{C})}{x+y+z} \quad (9)$$

where  $H(\text{Li}_x\text{B}_y\text{C}_z)$  is the total enthalpy of the  $\text{Li}_x\text{B}_y\text{C}_z$  compound.  $H(\text{Li})$ ,  $H(\text{B})$  and  $H(\text{C})$  are the enthalpy of the ground state of Li, B and C at 100 GPa. Here,  $H_d$  is introduced as the enthalpy above the convex hull to represent the relative stability on the phase diagram. Ground-state phases have  $H_d = 0$ .

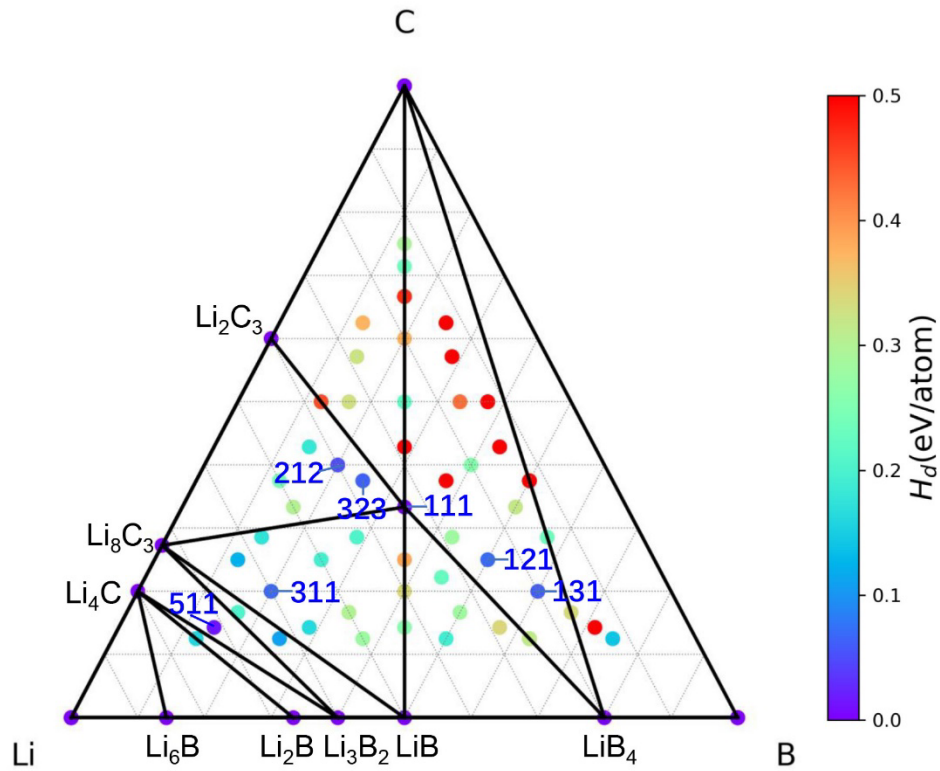


**Figure 1.** The convex hull of the Li-B-C system at 100 GPa.

As shown in Figure 1, LiBC is the only ternary ground-state compound at 100 GPa. The crystal structure is the same as the experimental structure of LiBC ( $P6_3/mmc$  symmetry) determined by Woerle *et al.* at ambient pressure [12]. This indicates that the ambient-pressure LiBC phase is stable up to 100 GPa, which agrees with previous

studies [58]. Figure 2(a) shows the atomic structure of hexagonal LiBC at 100 GPa. This structure is the same as the MgB<sub>2</sub> with alternating graphene-like B-C and Li layers. The detailed structural parameters are listed in Supplementary Table S2. The calculated phonon spectrum confirms that this phase is dynamically stable at 100 GPa (Figure S4 (a)). The electronic density of state (DOS) in Figure S4 (b) shows that LiBC is an insulating phase at 100 GPa.

Besides the ternary ground-state LiBC structure, we also identify a few low-enthalpy metastable structures with enthalpy very close to the convex hull ( $H_d < 100$  meV/atom), namely LiB<sub>2</sub>C, LiB<sub>3</sub>C, Li<sub>2</sub>BC<sub>2</sub>, Li<sub>3</sub>B<sub>2</sub>C<sub>3</sub>, Li<sub>3</sub>BC and Li<sub>5</sub>BC. The  $H_d$  are so small that these compounds [may be realized in experiments](#). We compute the Gibbs free energy of formation for one of the structures (LiB<sub>3</sub>C) to examine the effect of temperature on structural stability with the quasiharmonic approximation. The results suggest that the temperature may improve the stability of LiB<sub>3</sub>C (see Supplementary Note 2). The crystal structures of these Li-B-C compounds are shown in Figure 2(b)-(g). The LiB<sub>2</sub>C in Figure 2(b) adopts the orthorhombic structure with *Cmcm* symmetry. This structure is a 3D framework with PbO-type [59] layers of B<sub>2</sub> and C chains, separated by Li atoms, which is similar to *Cmcm* CeNiSi<sub>2</sub>. The *Cm* LiB<sub>3</sub>C also has a PbO-type layered motif of B<sub>3</sub>C, and Li atoms locate between two PbO-type layers as shown in Figure 2(c). This structure is similar to the BaFe<sub>2</sub>As<sub>2</sub> phase [60]. The Li<sub>2</sub>BC<sub>2</sub> (*Pbam*) and Li<sub>3</sub>B<sub>2</sub>C<sub>3</sub> (*Pm*) in Figure 2(d)-(e) both have B-C layered structures with five- and eight-membered rings and five-, six- and eight-membered rings, respectively. The *Cm* Li<sub>3</sub>BC (Figure 2(f)) is found to form B-C nanoribbons structure, while, for *P*-1 Li<sub>5</sub>BC (Figure 2(g)), B and C atoms connect to form chains. The structural parameters of these phases are listed in Supplementary Table S2. Figure S5-S10 show the phonon dispersions, and DOS for these metastable Li-B-C phases. The results show that, unlike the insulating LiBC, these low-enthalpy Li-B-C compounds are metallic. Furthermore, phonon calculations confirm that these Li-B-C compounds are dynamic stability at 100 GPa. It should be noted that the LiB<sub>3</sub>C structure has minor imaginary frequencies near the  $\Gamma$  point (Figure S6(a)). However, it does not mean the dynamical instability of this material. Since the phonon calculations are based on the harmonic approximation, the



presence of imaginary phonon frequencies may also be associated with a strongly anharmonic effect, which will be discussed later.

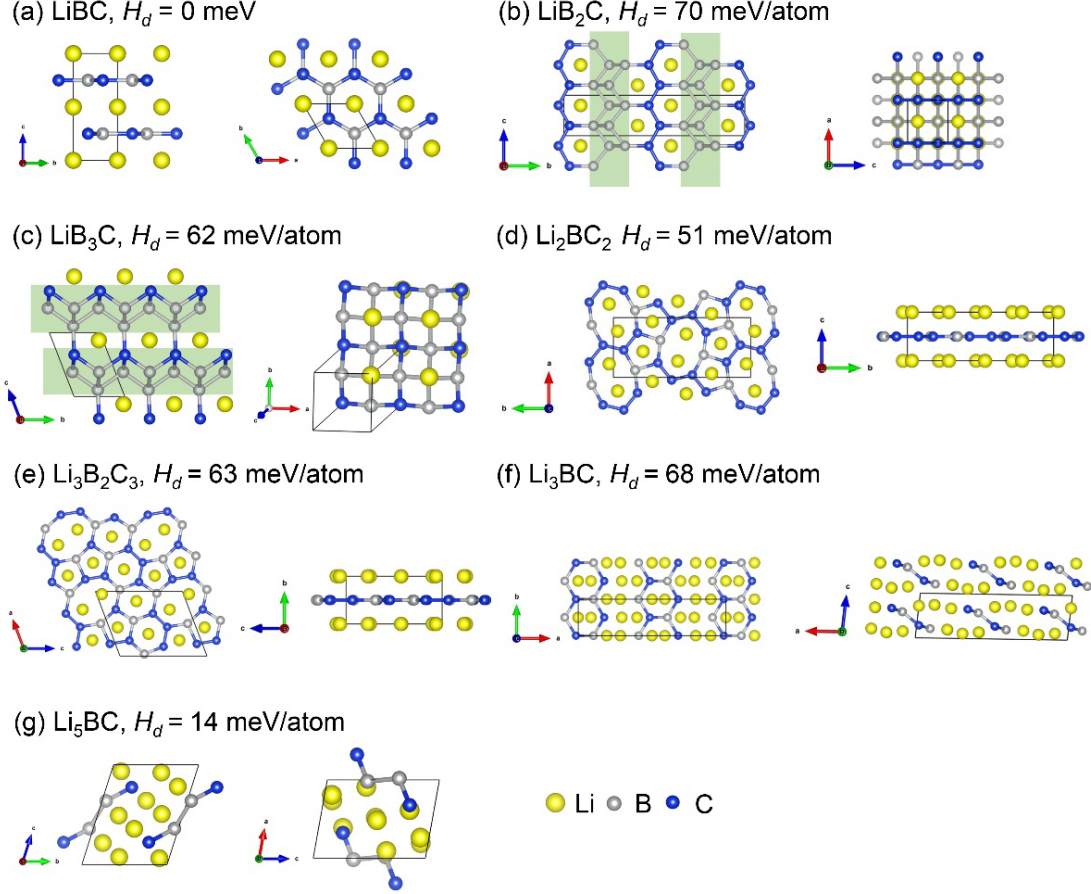


**Figure 2.** Atomic structures of (a)  $P6_3/mmc$   $\text{LiBC}$ , (b)  $Cmc$   $\text{LiB}_2\text{C}$ , (c)  $Cm$   $\text{LiB}_3\text{C}$ , (d)  $Pbam$   $\text{Li}_2\text{BC}_2$ , (e)  $Pm$   $\text{Li}_3\text{B}_2\text{C}_3$ , (f)  $Cm$   $\text{Li}_3\text{BC}$ , and (g)  $P-1$   $\text{Li}_5\text{BC}$  at 100 GPa. The light green rectangle denotes PbO-type motifs.

### 3.2 Fast screening of superconductivity of Li-B-C compounds

Motivated by the metallic properties of these metastable Li-B-C compounds, we further investigated their superconductivity. To determine the phonon-mediated superconductivity, it is usually based on the calculations of electron-phonon coupling in the full Brillouin zone. However, these calculations are time-consuming, particularly in complicated systems, which impedes the high-throughput superconducting material studies. Therefore we first employ a fast screening of these phases with the zone-center

EPC strength  $\lambda_{\Gamma}$  based on the frozen phonon method [29]. Here, the  $\lambda_{\Gamma}$  can be defined by

$$\lambda_{\Gamma v} = \frac{\tilde{\omega}_{\Gamma v}^2 - \omega_{\Gamma v}^2}{4\omega_{\Gamma v}^2}, \quad (10)$$

where the  $\omega_{\Gamma v}$  and  $\tilde{\omega}_{\Gamma v}$  are screened and unscreened phonon frequencies of mode  $v$  at zone-center, respectively. Using this method, we find only LiB<sub>3</sub>C has a high  $\sum_v \lambda_{\Gamma v}$  (the summation of zone-center EPC of all modes) as shown in Figure 3(a). The high  $\sum_v \lambda_{\Gamma v}$  of LiB<sub>3</sub>C can be attributed to the large difference between screened and unscreened phonon frequencies of mode 4 and mode 5 as shown in Figure 3(b).

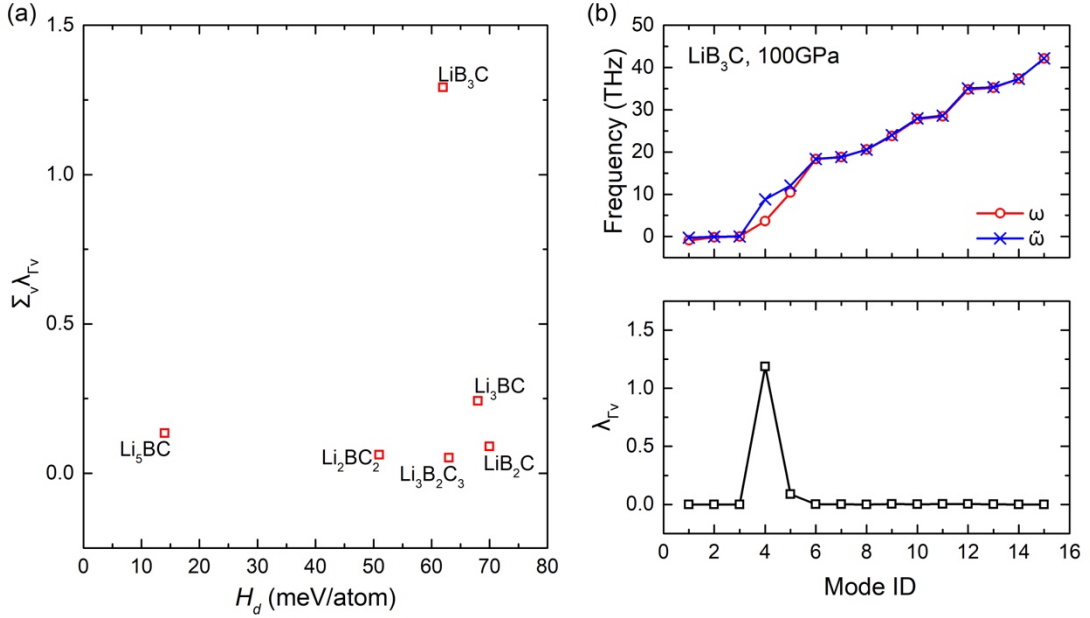


**Figure 3.** (a) The enthalpy above the convex hull ( $H_d$ ) versus EPC constant  $\sum_v \lambda_{\Gamma v}$  at the Brillouin zone center. (b) The screened and unscreened phonon frequency (top panel) and zone-center EPC strength (bottom panel) in LiB<sub>3</sub>C phase at 100 GPa.

To further quantify the electron-phonon interaction in LiB<sub>3</sub>C, we investigate its EPC with full Brillouin-zone calculations. Figure 4(a) shows the  $\gamma_{qv}$ -weighted phonon spectrum with DFPT calculations. Now one can see that phonon mode 4 and mode 5 have a large contribution to the phonon linewidth and correspondingly to the electron-phonon interaction near the  $\Gamma$  point, which agrees well with the fast screening results. These two modes mainly involve vibrations of boron and carbon atoms as shown in

Figure 4(b). Their vibrational configurations at the  $\Gamma$  point are shown in Figure 4(d) and Figure 4(e), respectively. Mode 4 corresponds to stretching vibrations of B2, B3, and C atoms in the  $a$ - $b$  plane. And for mode 5, B2-B3 atoms and B1-C atoms both show symmetric stretching vibrations in the  $a$ - $b$  plane. The calculated Eliashberg function  $\alpha^2F(\omega)$  is shown in Figure 4(c). The integrated EPC parameter  $\lambda$  is 1.40. The  $\omega_{\log}$  can be obtained from equation (8), which is 197.31 K. We predict  $T_c = 22$  K ( $\mu^* = 0.1$ ) for the  $\text{LiB}_3\text{C}$ . As a comparison, we also compute the full EPC for the  $\text{LiB}_2\text{C}$  phase with  $Cmcm$  symmetry, which is not expected to show a strong EPC from zone-center EPC calculations. We obtain  $\lambda = 0.37$  and  $T_c = 3$  K ( $\mu^* = 0.1$ ) for  $\text{LiB}_2\text{C}$  (see Figure S12), indicating the accuracy of the zone-center EPC screening method.

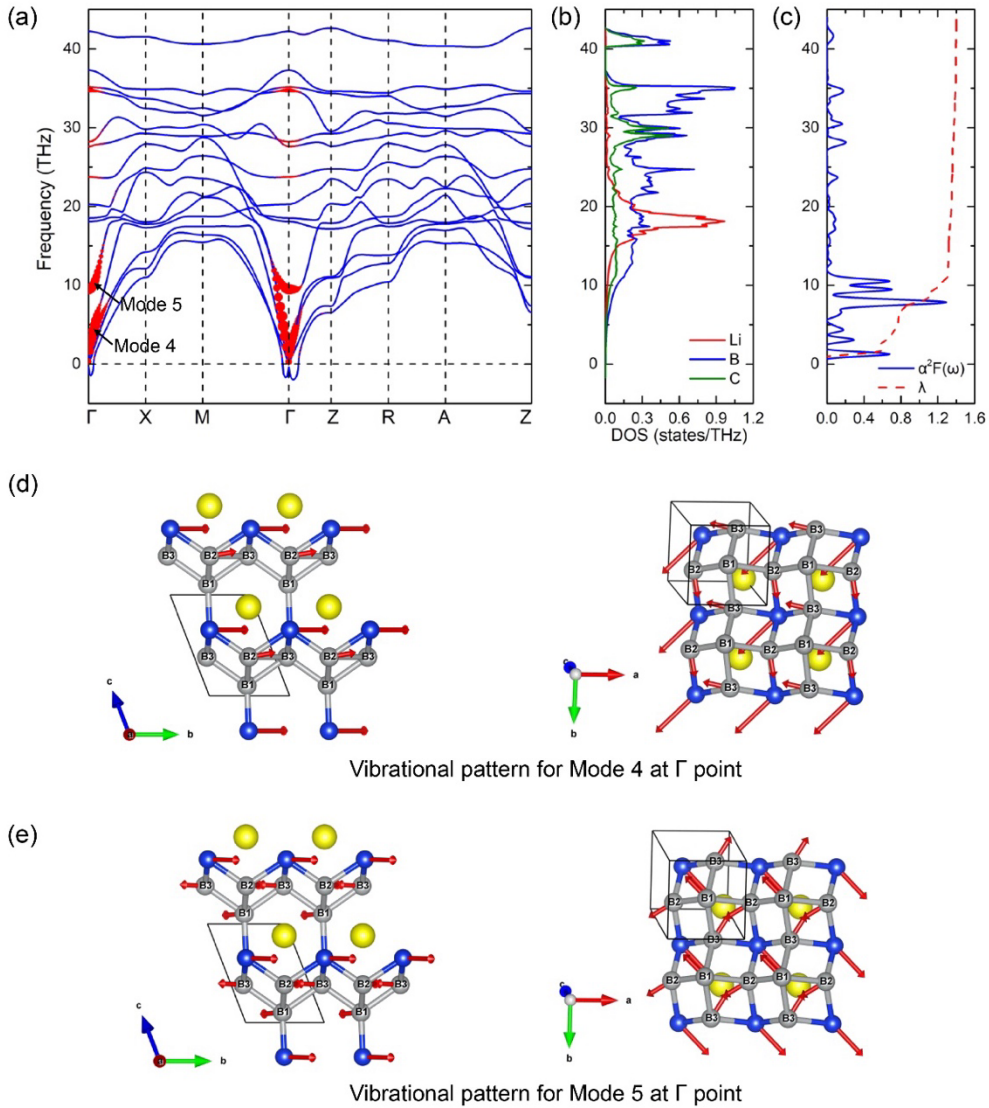


**Figure 4.** (a) Phonon spectrum of LiB<sub>3</sub>C. Red solid circles represent the phonon linewidth ( $\gamma_{qv}$ ) with a radius proportional to the strength. (b) projected phonon DOS. (c) Eliashberg spectral function  $\alpha^2F(\omega)$  with integrated EPC parameter  $\lambda(\omega)$ . The vibrational patterns for (d) mode 4 and (e) mode 5 at the  $\Gamma$  point.

### 3.3 Anharmonic effect of LiB<sub>3</sub>C

As mentioned above, there are small imaginary phonon frequencies contributed in LiB<sub>3</sub>C shown in Figure 4(a) and Figure S6(a). Specifically, we find the frequency of mode 4 shows a strong dependence on the magnitude of displacement in the frozen phonon calculations. To further investigate this behavior, we calculated the energy changes as all atoms displaced along the eigenmodes of mode 4 at the  $\Gamma$  point in Figure 5. The displacement for atom  $i$  is  $\mathbf{D}_i = u \frac{\mathbf{v}_i}{\sqrt{m_i}}$ , where  $u$  is the displacement amplitude,  $\mathbf{v}_i$  is the eigenvector,  $m_i$  is the atomic mass. To compare, we also plot mode 8, which is a harmonic mode mainly contributed by the Li vibration. Compared to the harmonic mode, the potential well of mode 4 is very flat at small displacement and increases rapidly at large displacement. It can only be fit to  $E(u) = A_2u^2 + A_4u^4$  with a vanishing  $A_2$  and a large  $A_4$  as shown in Figure 5(a). This indicates that mode 4 has unusually large anharmonicity and the conventional harmonic phonon calculations are in a nonperturbative regime. Therefore, the current harmonic energy, 1.10 THz or 4.56 meV, should be much lower than the actual energy. The correct treatment of anharmonic effects on superconductivity can be complicated. But such large anharmonicity has been seen previously and its influence on EPC and  $T_c$  has also been discussed in the literature [61, 62]. The EPC constant  $\lambda$  can be expected in general to be somewhat smaller. However, the influence of this change on  $T_c$  is not unique due to the significant increase of  $\omega_{\log}$  when the anharmonicity is included. Due to such cancellation effects, different formulas can produce the increase or decrease of  $T_c$ , however overall this effect seems to be small [61]. The phonon dispersions of LiB<sub>3</sub>C are also computed at 0 GPa and 50 GPa (see Figure S13). No negative frequency is found, suggesting that LiB<sub>3</sub>C is dynamically stable at low pressures.

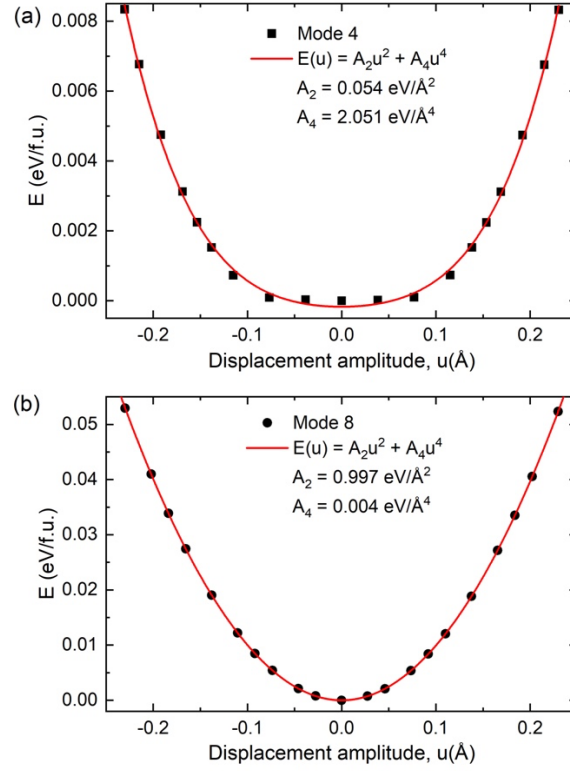


**Figure 5.** Frozen-phonon calculation of the total energy change as a function of atomic displacement for two zone-center modes. (a) The anharmonic mode 4 and (b) harmonic mode 8. The red curve shows the fitting.

## 4. Conclusions

In summary, we use the AGA method to study the Li-B-C system at 100 GPa. We identify several low-enthalpy metallic phases with stoichiometries of LiB<sub>2</sub>C, LiB<sub>3</sub>C, Li<sub>2</sub>BC<sub>2</sub>, Li<sub>3</sub>B<sub>2</sub>C<sub>3</sub>, Li<sub>3</sub>BC, and Li<sub>5</sub>BC. By a fast evaluation of zone-center electron-phonon interactions in these metallic Li-B-C structures, we identify that LiB<sub>3</sub>C can be a promising candidate for superconductivity. The calculations of EPC in the full Brillouin and analysis with Eliashberg function  $\alpha^2F(\omega)$  verify the superconductivity of LiB<sub>3</sub>C with EPC constant  $\lambda = 1.40$  and  $T_c = 22$  K. The electron-phonon interactions are mainly contributed by low-frequency anharmonic phonon modes involving vibrations of boron and carbon atoms. Our results indicate rich structural motifs in the Li-B-C system at high pressure, and the superconductivity in this system can happen in the phases without layered structure. This work also demonstrates an effective strategy to

combine crystal structure prediction and fast screening for conventional superconductors that can be used in many other systems.

## Acknowledgments

Work at Xiamen University was supported by the National Natural Science Foundation of China (11874307). R. Wang was supported by the Guangdong Basic and Applied Basic Research Foundation (Grant No. 2021A1515110328 & 2022A1515012174). Y. Sun and V. Antropov were supported by National Science Foundation Awards No. DMR-2132666. C.Z. Wang and F. Zhang were supported by the U.S. Department of Energy (DOE), Office of Science, Basic Energy Sciences, Materials Science and Engineering Division. Ames Laboratory is operated for the U.S. DOE by Iowa State University under Contract No. DE-AC02-07CH11358, including the grant of computer time at the National Energy Research Supercomputing Center (NERSC) in Berkeley.

## References

- [1] J. Nagamatsu, N. Nakagawa, T. Muranaka, Y. Zenitani, J. Akimitsu, *Nature*, **410**, 63 (2001).
- [2] Y. Kong, O.V. Dolgov, O. Jepsen, O.K. Andersen, *Phys Rev B*, **64**, 020501 (2001).
- [3] T. Yildirim, O. Gulseren, J.W. Lynn, C.M. Brown, T.J. Udovic, Q. Huang, N. Rogado, K.A. Regan, M.A. Hayward, J.S. Slusky, et al., *Phys Rev Lett*, **87**, 037001 (2001).
- [4] N. Emery, C. Herold, M. d'Astuto, V. Garcia, C. Bellin, J.F. Mareche, P. Lagrange, G. Loupiau, *Phys Rev Lett*, **95**, 087003 (2005).
- [5] M. Gao, X.-W. Yan, Z.-Y. Lu, T. Xiang, *Phys Rev B*, **101**, 094501 (2020).
- [6] E. Haque, M.A. Hossain, C. Stampfl, *Phys Chem Chem Phys*, **21**, 8767 (2019).
- [7] T. Bazhiron, Y. Sakai, S. Saito, M.L. Cohen, *Physical Review B*, **89**, 045136 (2014).
- [8] T.E. Weller, M. Ellerby, S.S. Saxena, R.P. Smith, N.T. Skipper, *Nature Physics*, **1**, 39 (2005).
- [9] W. Hayami, T. Tanaka, *Aip Advances*, **10**, 065213 (2020).
- [10] J.M. An, W.E. Pickett, *Phys Rev Lett*, **86**, 4366 (2001).
- [11] S. Di Cataldo, S. Qulaghasi, G.B. Bachelet, L. Boeri, *Phys Rev B*, **105**, 064516 (2022).
- [12] M. Worle, R. Nesper, G. Mair, M. Schwarz, H.G. Vonschnering, *Z Anorg Allg Chem*, **621**, 1153 (1995).
- [13] P.F. Karimov, N.A. Skorikov, E.Z. Kurmaev, L.D. Finkelstein, S. Leitch, J. MacNaughton, A. Moewes, T. Mori, *J Phys-Condens Mat*, **16**, 5137 (2004).
- [14] J. Bardeen, L.N. Cooper, J.R. Schrieffer, *Physical Review*, **108**, 1175 (1957).
- [15] H. Rosner, A. Kitaigorodsky, W.E. Pickett, *Physical Review Letters*, **88**, 127001 (2002).
- [16] A. Bharathi, S.J. Balaselvi, M. Premila, T.N. Sairam, G.L.N. Reddy, C.S. Sundar, Y. Hariharan, *Solid State Commun*, **124**, 423 (2002).

- 
- 1 [17] D. Souptel, Z. Hossain, G. Behr, W. Loser, C. Geibel, Solid State Commun, **125**, 17 (2003).
  - 2 [18] A.M. Fogg, P.R. Chalker, J.B. Claridge, G.R. Darling, M.J. Rosseinsky, Phys Rev B, **67**, 245106
  - 3 (2003).
  - 4 [19] A.M. Fogg, J.B. Claridge, G.R. Darling, M.J. Rosseinsky, Chem Commun, **12**, 1348 (2003).
  - 5 [20] A.M. Fogg, J. Meldrum, G.R. Darling, J.B. Claridge, M.J. Rosseinsky, J Am Chem Soc, **128**,
  - 6 10043 (2006).
  - 7 [21] R. Miao, J. Yang, M. Jiang, Q. Zhang, D. Cai, C. Fan, Z. Bai, C. Liu, F. Wu, S. Ma, Journal of
  - 8 Applied Physics, **113**, 133910 (2013).
  - 9 [22] M. Gao, Z.Y. Lu, T. Xiang, Phys Rev B, **91**, 045132 (2015).
  - 10 [23] Y. Quan, W.E. Pickett, Phys Rev B, **102**, 144504 (2020).
  - 11 [24] A.P. Drozdov, P.P. Kong, V.S. Minkov, S.P. Besedin, M.A. Kuzovnikov, S. Mozaffari, L. Balicas,
  - 12 F.F. Balakirev, D.E. Graf, V.B. Prakapenka, et al., Nature, **569**, 528 (2019).
  - 13 [25] A.P. Drozdov, M.I. Eremets, I.A. Troyan, V. Ksenofontov, S.I. Shylin, Nature, **525**, 73 (2015).
  - 14 [26] M. Somayazulu, M. Ahart, A.K. Mishra, Z.M. Geballe, M. Baldini, Y. Meng, V.V. Struzhkin, R.J.
  - 15 Hemley, Physical Review Letters, **122**, 027001 (2019).
  - 16 [27] E. Snider, N. Dasenbrock-Gammon, R. McBride, X. Wang, N. Meyers, K.V. Lawler, E. Zurek, A.
  - 17 Salamat, R.P. Dias, Phys Rev Lett, **126**, 117003 (2021).
  - 18 [28] H.K. Mao, X.J. Chen, Y. Ding, B. Li, L. Wang, Rev Mod Phys, **90**, 015007 (2018).
  - 19 [29] Y. Sun, F. Zhang, C.-Z. Wang, K.-M. Ho, I.I. Mazin, V. Antropov, Physical Review Materials, **6**,
  - 20 074801 (2022).
  - 21 [30] S.Q. Wu, M. Ji, C.Z. Wang, M.C. Nguyen, X. Zhao, K. Umemoto, R.M. Wentzcovitch, K.M. Ho,
  - 22 J Phys Condens Matter, **26**, 035402 (2014).
  - 23 [31] S.M. Foiles, M.I. Baskes, M.S. Daw, Phys Rev B Condens Matter, **33**, 7983 (1986).
  - 24 [32] P. Brommer, F. Gahler, Philos Mag, **86**, 753 (2006).
  - 25 [33] P. Brommer, F. Gahler, Model Simul Mater Sc, **15**, 295 (2007).
  - 26 [34] G. Kresse, D. Joubert, Phys Rev B, **59**, 1758 (1999).
  - 27 [35] G. Kresse, J. Furthmuller, Phys Rev B, **54**, 11169 (1996).
  - 28 [36] G. Kresse, J. Furthmuller, Comp Mater Sci, **6**, 15 (1996).
  - 29 [37] J.P. Perdew, K. Burke, M. Ernzerhof, Phys Rev Lett, **77**, 3865 (1996).
  - 30 [38] S. Froyen, Phys Rev B Condens Matter, **39**, 3168 (1989).
  - 31 [39] A. Togo, F. Oba, I. Tanaka, Phys Rev B, **78**, 134106 (2008).
  - 32 [40] A. Togo, I. Tanaka, Scripta Mater, **108**, 1 (2015).
  - 33 [41] P. Giannozzi, S. Baroni, N. Bonini, M. Calandra, R. Car, C. Cavazzoni, D. Ceresoli, G.L.
  - 34 Chiarotti, M. Cococcioni, I. Dabo, et al., J Phys Condens Matter, **21**, 395502 (2009).
  - 35 [42] P. Giannozzi, O. Andreussi, T. Brumme, O. Bunau, M.B. Nardelli, M. Calandra, R. Car, C.
  - 36 Cavazzoni, D. Ceresoli, M. Cococcioni, et al., J Phys-Condens Mat, **29**, 465901 (2017).
  - 37 [43] S. Baroni, S. de Gironcoli, A. Dal Corso, P. Giannozzi, Rev Mod Phys, **73**, 515 (2001).
  - 38 [44] A. Dal Corso, Comp Mater Sci, **95**, 337 (2014).
  - 39 [45] G.M. Eliashberg, Sov. Phys. JETP, **11**, 696 (1960).
  - 40 [46] G.M. Eliashberg, Sov. Phys. JETP, **12**, 1000 (1961).
  - 41 [47] P.B. Allen, Phys Rev B, **6**, 2577 (1972).
  - 42 [48] P.B. Allen, R.C. Dynes, Phys Rev B, **12**, 905 (1975).
  - 43 [49] C.F. Richardson, N.W. Ashcroft, Phys Rev Lett, **78**, 118 (1997).
  - 44 [50] K.H. Lee, K.J. Chang, M.L. Cohen, Phys Rev B Condens Matter, **52**, 1425 (1995).

- 
- 1 [51] J. Lv, Y. Wang, L. Zhu, Y. Ma, Phys Rev Lett, **106**, 015503 (2011).  
2 [52] C.J. Pickard, R.J. Needs, Phys Rev Lett, **102**, 146401 (2009).  
3 [53] A.R. Oganov, J.H. Chen, C. Gatti, Y.Z. Ma, Y.M. Ma, C.W. Glass, Z.X. Liu, T. Yu, O.O.  
4 Kurakevych, V.L. Solozhenko, Nature, **457**, 863 (2009).  
5 [54] T. Yamanaka, S. Morimoto, Acta Crystallogr B, **52**, 232 (1996).  
6 [55] F. Peng, M. Miao, H. Wang, Q. Li, Y. Ma, J Am Chem Soc, **134**, 18599 (2012).  
7 [56] A. Hermann, A. McSorley, N.W. Ashcroft, R. Hoffmann, J Am Chem Soc, **134**, 18606 (2012).  
8 [57] A. Jay, O.H. Duparc, J. Sjakste, N. Vast, Journal of Applied Physics, **125**, 185902 (2019).  
9 [58] M.G. Zhang, Europhys. Lett, **114**, 16001 (2016).  
10 [59] D.E. Bugaris, M. Sturza, F. Han, J. Im, D.Y. Chung, A.J. Freeman, M.G. Kanatzidis, European  
11 Journal of Inorganic Chemistry, **2015**, 2164 (2015).  
12 [60] F. Rullier-Albenque, D. Colson, A. Forget, P. Thuéry, S. Poissonnet, Phys Rev B, **81**, 224503  
13 (2010).  
14 [61] M. Dogan, S. Oh, M.L. Cohen, Phys Rev B, **105**, L020509 (2022).  
15 [62] A.M. Shipley, M.J. Hutcheon, R.J. Needs, C.J. Pickard, Physical Review B, **104**, 054501 (2021).